Journal of Zhejiang University SCIENCE A
ISSN 1673-565X (Print); ISSN 1862-1775 (Online)
www.zju.edu.cn/jzus; www.springerlink.com
E-mail: jzus@zju.edu.cn

Numerical simulation of a gas pipeline network using computational fluid dynamics simulators

SELEZNEV Vadim

(*Physical and Technical Center, Joint Stock Company, Sarov, 607180, Russia*)

E-mail: sve@ptc.sar.ru

Received Aug. 19, 2006; revision accepted Dec. 15, 2006

Abstract: This article describes numerical simulation of gas pipeline network operation using high-accuracy computational fluid dynamics (CFD) simulators of the modes of gas mixture transmission through long, multi-line pipeline systems (CFD-simulator). The approach used in CFD-simulators for modeling gas mixture transmission through long, branched, multi-section pipelines is based on tailoring the full system of fluid dynamics equations to conditions of unsteady, non-isothermal processes of the gas mixture flow. Identification, in a CFD-simulator, of safe parameters for gas transmission through compressor stations amounts to finding the interior points of admissible sets described by systems of nonlinear algebraic equalities and inequalities. Such systems of equalities and inequalities comprise a formal statement of technological, design, operational and other constraints to which operation of the network equipment is subject. To illustrate the practicability of the method of numerical simulation of a gas transmission network, we compare computation results and gas flow parameters measured on-site at the gas transmission enterprise.

Key words: Long branched gas pipeline network, Unsteady, Non-isothermal gas flow, CFD-simulator, Numerical simulation, Finite Volume Method, Interior Point Method

doi:10.1631/jzus.2007.A0755 **Document code:** A **CLC number:** TU373

INTRODUCTION

At the present level of development of long, branched gas transmission networks (GTN), solving the problems of improving safety, efficiency and environmental soundness of operation of industrial pipeline systems calls for the application of methods of numerical simulation (Seleznev and Aleshin, 2004). The development of automated devices for technical inspection and process control, and availability of high-performance computer hardware have created a solid technical basis to introduce numerical simulation methods into the industrial practice of GTN analysis and operation. The above methods became especially worthy in view of GTN ageing accompanied by increasing number of accidents (Kinsman and Lewis, 2000; True, 2001). One of the promising approaches for numerical analysis of GTN operating at industrial energy plants is the development and application of high-accuracy computational fluid dynamic (CFD) simulators of modes of gas mixture transmission through long, branched pipeline systems (CFD-simulator) (Seleznev *et al*., 2005a).

GENERAL CHARACTERISTIC OF A CFD-SIMULATOR

Actually, a CFD-simulator is a special-purpose software simulating, in "online" and "real time" modes with a high similarity and in sufficient detail, the physical processes of gas mixture transmission through a particular GTN. The development of a CFD-simulator focuses much attention to correctness of simulation of gas flows in the pipelines and to the impact produced by operation of relevant GTN gas pumping equipment (including gas compressor unit (GCU), valves, gas pressure reducers, etc.) and the

environment upon the physical processes under study.

From the standpoint of mathematical physics, a CFD-simulator performs numerical simulation of unsteady, non-isothermal processes of a gas mixture flow in long, branched, multi-line gas pipeline systems. Such simulation is aimed at obtaining high-accuracy estimates of the actual distribution (over time and space) of fluid dynamics parameters for the full range of modes of gas mixture transmission through the specific GTN in normal and emergency conditions of its operation, as well as of the actual (temporal) distribution of main parameters of GTN equipment operation, which can be expressed as functional dependencies on the specified control actions on the GTN and corresponding boundary conditions. Theoretically, the high-accuracy of estimates of gas flow parameters is achieved here due to:

(1) minimization of the number and depth of accepted simplifications and assumptions in the mathematical modeling of gas flows through long, branched, multi-section pipelines and gas compressor stations (CS) on the basis of adaptation of complete basic fluid dynamics models;

(2) minimization of the number and depth of accepted simplifications and assumptions in the construction of a computational model of the simulated GTN;

(3) improving methods for numerical analysis of the constructed mathematical models based upon results of theoretical investigation of their convergence and evaluation of possible errors of solution;

(4) taking into account the mutual influence of GTN components in the simulation of its operation;

(5) detailed analysis and mathematically formal description of the technologies and supervisor procedures for management of gas mixture transport at the simulated GTN;

(6) automated mathematic filtration of occasional and systemic errors in input data, etc.

Input information required for work of a CFD-simulator is delivered from the Supervisory Control and Data Acquisition System (SCADA-system) operated at the simulated GTN.

CFD-simulator's operating results are used for on-line control of the specific GTN, as well as in short-term and long-term forecasts of optimal and safe modes of gas mixture transport subject to fulfillment of contractual obligations. Also, a CFD-simulator is often used as base software for a hardware and software system for prevention or early detection of GTN failures.

STRUCTURE OF A CFD-SIMULATOR

For better illustration of the material presented in this article, but without losing the generality of reasoning, further description of a CFD-simulator will be based on a sample pipeline network of a gas transmission enterprise. For the purpose of modeling, natural gas is deemed to be a homogenous gas mixture.

A CFD-simulator of a gas transmission enterprise's GTN is created by combining CS mathematical models into a single model of the enterprise's pipeline system, by applying models of multi-line gas pipelines segments (GPS) (Fig.1a) (Seleznev *et al*., 2003). At that, in accordance with their process flow charts, the CS models are created by combining of GCU, dust catcher (DC) and air cooling device (ACD) models by applying mathematical models of connecting gas pipelines (CGP) (Fig.1b).

In a CFD-simulator, the control of simulated natural gas transmission through the GTN is provided by the following control commands: alteration of shaft rotation frequency of centrifugal superchargers

(a)

(b)

Fig.1 Example of a multi-line GPS (a) and CGP of a CS (b)

(CFS) of GCU or their startup/shutdown; opening or closing of valves at a CS and valve platforms of multi-line GPS; alteration of the rates of gas consumption by industrial enterprises and public facilities; alteration of the gas reduction program at reduction units; alteration of the operation program at gas distributing stations; change in the program of ACD operating modes, etc. Therefore, simulated control in a CFD-simulator adequately reflects the actual control of natural gas transmission through pipeline networks of the gas transmission enterprise.

Generally, a CFD-simulator can be divided into three interrelated components (elements) (Seleznev *et al*., 2005b). Each of these components is an integral part of the CFS-simulator.

The first system element is a computational scheme of a gas transmission enterprise pipeline system built on the basis of typical segments representing minimum distinctions from a comprehensive topology of an actual system considering the arrangement of valves, the system architecture, laying conditions, the process flow scheme of the system's CS, etc. The second component is a database containing input and operative (current) data on time-dependent (owing to valves operation) system topology, pipeline parameters, process modes and natural gas transmission control principles for an actual gas transmission enterprise. The third component of a CFD-simulator is a mathematical software which operates the first two CFD-simulator elements and is designed for:

(1) the building of computational schemes based on the input data in database (multi-line GPS, individual CS or gas transmission enterprise pipeline system) with minimum distinctions from the topology of actual pipeline systems, system architecture, laying conditions, process flow chart, etc.;

(2) the numerical analysis of computational schemes based on the input and operative data and considering the process modes and natural gas transmission principles adopted in this enterprise.

The mathematical software includes (in addition to the computation core) a user interface environment imitating the operation of actual control panels located at gas transmission enterprises control centers in a visual form familiar to operators. This provides for faster training and, for the operator, easier adaptation to the CFD-simulator.

A typical example of a CFD-simulator is the AMADEUS CFD-simulator developed from the Alfargus/PipeFlow software and launched into operation for solving industrial tasks of the Control Center of the SPP International Gas Transmission Company (Slovakia) at the beginning of this century (Seleznev *et al*., 2005a).

SIMULATION OF MULTI-LINE GPS BY MATHEMATICAL SOFTWARE OF A CFD-SIMULATOR

For numerical evaluation of parameters of unsteady, non-isothermal processes of the gas mixture flow in multi-line GPS, a CFD-simulator uses a model developed by tailoring the full set of integral fluid dynamics equations to conditions of the gas flow through long branched pipeline systems. Transformation of the 3D integral problem to an equivalent one-dimensional differential problem is implemented by accepting the minimum of required simplifications and projecting the initial system of equations onto the pipeline's geometrical axis. Special attention is given to the adequacy of simulation of pipeline junction nodes where the 3D nature of the gas flow is vividly displayed.

To give an example of results of such transforms, it is expedient to present a fluid dynamics model of a transient non-isothermal turbulent flow of a viscous, chemically inert, compressible, multi-component heat-conductive gas mixture through multi-line GPS consisting of round cross-sections pipes and rigid rough heat-conductive walls (Seleznev *et al*., 2005a):

(1) For each pipe adjacent to the junction node:

$$\frac{\partial(\rho f)}{\partial t}+\frac{\partial}{\partial x}(\rho w f)=0; \tag{1}$$

$$\frac{\partial}{\partial t}(\rho Y_m f)+\frac{\partial}{\partial x}(\rho Y_m w f)-\frac{\partial}{\partial x}\left(\rho f D_m \frac{\partial Y_m}{\partial x}\right)=0,$$

$$m=1,\ldots,N_S-1,\quad Y_{N_S}=1-\sum_{m=1}^{N_S-1}Y_m; \tag{2}$$

$$\frac{\partial(\rho w f)}{\partial t}+\frac{\partial(\rho w^2 f)}{\partial x} =-f\left(\frac{\partial p}{\partial x}+g\rho\frac{\partial z_1}{\partial x}\right)-\frac{\pi}{4}\lambda\rho w|w|R; \tag{3}$$

$$\frac{\partial}{\partial t}\left[\rho f\left(\varepsilon+\frac{w^2}{2}\right)\right]+\frac{\partial}{\partial x}\left[\rho w f\left(\varepsilon+\frac{w^2}{2}\right)\right]$$
$$=-\frac{\partial}{\partial x}(pwf)-\rho w f g\frac{\partial z_1}{\partial x}-p\frac{\partial f}{\partial t}+Qf+\frac{\partial}{\partial x}\left(kf\frac{\partial T}{\partial x}\right)$$
$$-\Phi(T,T_{\mathrm{am}})+\frac{\partial}{\partial x}\left(\rho f\sum_{m=1}^{N_S}\left(\varepsilon_m D_m\frac{\partial Y_m}{\partial x}\right)\right); \tag{4}$$

(2) For each of the junction nodes (the Pryalov model):

$$\frac{\partial\rho}{\partial t}+\sum_{n=1}^{N}{}^{(n)}\Theta\,{}^{(n)}\left(\frac{\partial(\rho w)}{\partial x}\right)=0; \tag{5}$$
$$\frac{\partial(\rho Y_m)}{\partial t}+\sum_{n=1}^{N}{}^{(n)}\left(\frac{\partial(\rho Y_m w)}{\partial x}\right){}^{(n)}\Theta$$
$$-\sum_{n=1}^{N}{}^{(n)}\left[\frac{\partial}{\partial x}\left(\rho D_m\frac{\partial Y_m}{\partial x}\right)\right]{}^{(n)}\Theta=0,$$
$$m=1,\ldots,N_S-1,$$
$${}^{(n)}Y_{N_S}=1-\sum_{m=1}^{N_S-1}{}^{(n)}Y_m; \tag{6}$$
$${}^{(n)}\frac{\partial(\rho w)}{\partial t}+{}^{(n)}\frac{\partial(\rho w^2)}{\partial x}$$
$$=-{}^{(n)}\left(\frac{\partial p}{\partial x}\right)-g\rho\,{}^{(n)}\left(\frac{\partial z_1}{\partial x}\right)-\frac{1}{4\,{}^{(n)}R}{}^{(n)}(\lambda\rho w|w|),$$
$$n=1,\ldots,N; \tag{7}$$
$$\frac{\partial(\rho\varepsilon)}{\partial t}+\sum_{n=1}^{N}{}^{(n)}\left(\frac{\partial(\rho\varepsilon w)}{\partial x}\right){}^{(n)}\Theta$$
$$=-\sum_{n=1}^{N}{}^{(n)}p\,{}^{(n)}\left(\frac{\partial w}{\partial x}\right){}^{(n)}\Theta+\frac{1}{4}\sum_{n=1}^{N}\frac{1}{{}^{(n)}R}\,{}^{(n)}\lambda\,{}^{(n)}\rho\,{}^{(n)}|w|^3\,{}^{(n)}\Theta$$
$$+Q+\sum_{n=1}^{N}{}^{(n)}\frac{\partial}{\partial x}\left(k\frac{\partial T}{\partial x}\right){}^{(n)}\Theta-\sum_{n=1}^{N}\frac{{}^{(n)}\Phi(T,T_{\mathrm{am}})}{{}^{(n)}f}\,{}^{(n)}\Theta$$
$$+\sum_{n=1}^{N}\sum_{m=1}^{N_S}{}^{(n)}\frac{\partial}{\partial x}\left(\rho\varepsilon_m D_m\frac{\partial Y_m}{\partial x}\right){}^{(n)}\Theta; \tag{8}$$
$${}^{(n)}T={}^{(\xi)}T,\ \varepsilon={}^{(n)}\varepsilon={}^{(\xi)}\varepsilon,\ {}^{(n)}(\varepsilon_m)={}^{(\xi)}(\varepsilon_m),$$
$$\rho={}^{(n)}\rho={}^{(\xi)}\rho,\ {}^{(n)}p={}^{(\xi)}p,\ {}^{(n)}k={}^{(\xi)}k,$$
$${}^{(n)}(D_m)={}^{(\xi)}(D_m),\ Y_m={}^{(n)}(Y_m)={}^{(\xi)}(Y_m),$$
$${}^{(n)}Q={}^{(\xi)}Q,\ {}^{(n)}(z_1)={}^{(\xi)}(z_1),$$
$$\text{for any } n,\xi\in\overline{1,N} \text{ and } m\in\overline{1,N_S}; \tag{9}$$
$$\sum_{n=1}^{N}{}^{(n)}w\,{}^{(n)}f\,{}^{(n)}s=0;\ \sum_{n=1}^{N}{}^{(n)}\left(\frac{\partial T}{\partial x}\right){}^{(n)}f\,{}^{(n)}s=0;$$
$$\sum_{n=1}^{N}{}^{(n)}\left(\frac{\partial Y_m}{\partial x}\right){}^{(n)}f\,{}^{(n)}s=0; \tag{10}$$
$${}^{(n)}s=-({}^{(0)}\boldsymbol{n}\,{}^{(n)}\boldsymbol{i})=\begin{cases}1, \text{ if } ({}^{(0)}\boldsymbol{n}\,{}^{(n)}\boldsymbol{i})<0;\\ -1, \text{ if } ({}^{(0)}\boldsymbol{n}\,{}^{(n)}\boldsymbol{i})>0,\end{cases}$$
$${}^{(n)}\Theta=\frac{{}^{(n)}f_L}{\sum_{k=1}^{N}{}^{(k)}f_L},\ 0<{}^{(n)}\Theta<1,\ \sum_{n=1}^{N}{}^{(n)}\Theta=1; \tag{11}$$

(3) Equation of state (EOS) and additional correlations:

$$p=p(\{S_{\mathrm{mix}}\});\ \varepsilon=\varepsilon(\{S_{\mathrm{mix}}\});\ k=k(\{S_{\mathrm{mix}}\});$$
$$\varepsilon_m=\varepsilon_m(\{S_{\mathrm{mix}}\});\ D_m=D_m(\{S_{\mathrm{mix}}\}); \tag{12}$$
$$m=1,\ldots,N_S;\ T_1=T_2=\ldots=T_{N_S}.$$

where ρ is the density of the gas mixture; f is the flow cross-sectional area of pipeline; t is time (marching variable); x is the spatial coordinate over the pipeline's geometrical axis (spatial variable); w is the projection of the pipeline flow cross-section averaged vector of the mixture velocity on the pipeline's geometrical axis (on the assumption of the developed turbulence); Y_m is relative mass concentration of the m component of the gas mixture; D_m is binary diffusivity of component m in the residual mixture; N_S is the number of components of the homogeneous gas mixture; p is the pressure in the gas mixture; g is gravitational acceleration modulus; z_1 is the coordinate of the point on the pipeline's axis, measured, relative to an arbitrary horizontal plane, upright; π is the Pythagorean number; λ is the friction coefficient in the Darcy-Weisbach formula; $R=\sqrt{f/\pi}$ is the pipe's internal radius; ε is specific (per unit mass) internal energy of the gas mixture; Q is specific (per unit volume) heat generation rate of sources; k is thermal conductivity; T is the temperature of gas mixture; ε_m is specific (per unit mass) internal energy of the m component; T_m is the temperature of the m component; N is the number of pipes comprising one junction (see Eqs.(5)~(11)); ${}^{(n)}s$, ${}^{(n)}\Theta$ are auxiliary functions (re ${}^{(0)}\boldsymbol{n}$, ${}^{(n)}\boldsymbol{i}$ see Fig.3b below); $\{S_{\mathrm{mix}}\}$ is a set of parameters of gas mixture. Function $\Phi(T,T_{\mathrm{am}})$ is defined by the law of heat transfer from the pipe to the environment and expresses the aggregate heat flow through the pipe walls along perimeter χ of the flow

cross-section with area f ($\Phi(T,T_{am})>0$ is cooling), T_{am} is the ambient temperature. To denote the relationship of a value to the pipe numbered by n, we use a parenthesized superscript on the left side of the value, e.g.: ${}^{(n)}\rho$. In Eqs.(1)~(12), we use physical magnitudes averaged across the pipeline's flow cross-section. The set of Eqs.(1)~(12) is supplemented by the boundary conditions and conjugation conditions. As conjugation conditions it is possible to specify boundary conditions simulating a complete rupture of the pipeline and/or its shutoff, operation of valves, etc.

As was stated above, the energy Eqs.(4)~(8) comprise function $\Phi(T,T_{am})$ describing the heat exchange between the environment and natural gas in the course of its pipeline transmission. The space-time distribution of function $\Phi(T,T_{am})$ is defined, in the CFD-simulator, at specified time steps of the numerical analysis of parameters of the transient mode of gas transmission by solving a series of conjugate 2D or 3D problems of heat exchange between the gas flow core and the environment. At that, calculations are made for preselected limited segments of the pipeline, surrounded by media with known thermophysical properties. To illustrate the above, Fig.2a gives an example of a cross-section geometry of a simplified computational domain in case of a conjugate thermal problem. Fig.2a uses the following notations: D_1 is the insulation outside diameter; D_2 is the pipeline inside diameter; H_1 is the soil depth, for which the temperature is prescribed; H_2 is the distance between the pipeline axis and the ground surface.

Such analysis results in evaluations of the aggregate heat flow $\Phi(T,T_{am})$ and corresponding evaluations of parameters of the gas flow through the pipe. Such segregation is permissible due to the significant differences in the dynamics of these values' changing over time. The approximation of results of calculations of the aggregate heat flow for the entire pipeline's length and for intermediate time steps of the gas flow numerical simulation uses, as a rule, polynominal functions.

To solve conjugate 2D or 3D problems of heat exchange between the gas flow core and the environment, it is possible to use, for instance, the Finite Element Method (FEM). The pattern of a typical temperature field around a pipeline obtained by the Alfargus computer-based analytical system using the FEM is shown in Fig.2b.

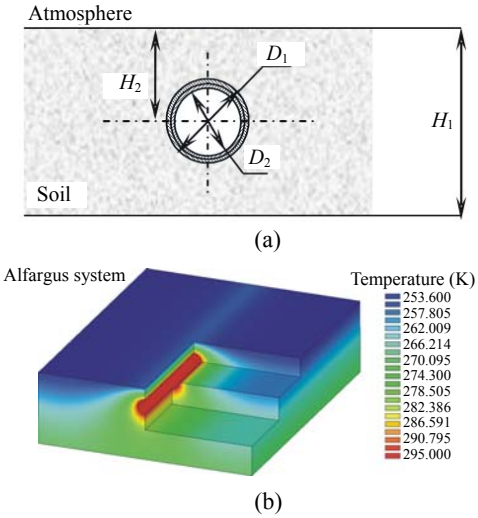

Fig.2 Computational domain for thermal analysis of the gas pipeline (a) and example of the temperature field around the gas pipeline (b)

In order to improve the adequacy of simulation of gas flows at a pipeline junction in the construction of a subsystem of Eqs.(5)~(11), we used the geometrical model of a junction (Fig.3) proposed by S. Pryalov (Seleznev *et al*., 2005a).

In this model, volume ${}^{(0)}V$ can be depicted as a

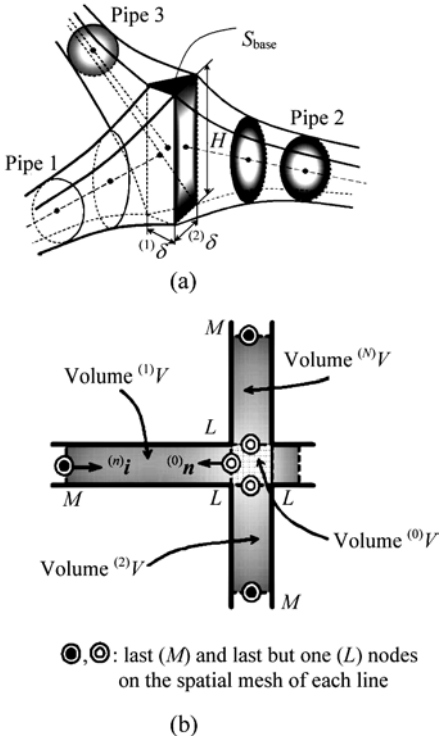

Fig.3 A schematic of a pipeline junction. (a) 3D drawing; (b) Diagram

right prism with base area S_{base} and height H (Fig.3a). For the prism lateral surface with linear dimensions ${}^{(n)}\delta$, relation is: ${}^{(n)}\delta={}^{(n)}f/H$, where ${}^{(n)}f$ is the cross-sectional area of the pipe adjacent to the junction core ${}^{(0)}V$. It should be noted that the summarized volume of the joint is equal to $V=\bigcup_{n=1}^{N}{}^{(n)}V$, where ${}^{(n)}V$, n=1,…,N, is the volume of an infinitely small section of the pipe adjacent to the junction core ${}^{(0)}V$ (Fig.3b). The prism base area can be represented as follows: $S_{base}=\varsigma_{base}{}^{(1)}\delta^2$, where ς_{base} is the factor depending on the prism base geometry only. Now volume ${}^{(0)}V$ can be determined by the following formula: ${}^{(0)}V=HS_{base}=H\varsigma_{base}\left(\frac{{}^{(1)}f}{H}\right)^2=\frac{\varsigma_{base}{}^{(1)}f^2}{H}$, which means that $\lim\limits_{H\to\infty}{}^{(0)}V=\lim\limits_{H\to\infty}\frac{\varsigma_{base}{}^{(1)}f^2}{H}=0$. The application of this geometrical model enabled us to approximate compliance with mass, momentum and energy conservation laws at the pipelines junction.

The mathematical model of gas transmission Eqs.(1)~(12) includes EOS Eq.(12). As is well known, the most theoretically proven form of a thermal EOS of gas is the virial EOS:

$$\frac{pV}{RT}=1+\frac{B}{V}+\frac{C}{V^2}+..., \tag{13}$$

where V is the volume of one gas mole, cm^3/mole; R is the gas constant, which has different values for different contents of natural gas being transmitted through pipelines; B (cm^3/mole), C (cm^6/mole^2), …, are the second, third, etc. virial coefficients depending on gas temperature and being independent of gas pressure and density. In the case of low gas density ($V\to\infty$), EOS Eq.(13) is transformed into the Clapeyron equation of state. Let us note that the second, third, etc. terms of Eq.(13) describe the allowance for gas non-ideality which results from the double, triple, etc. interaction of gas particles, respectively.

Apart from Eq.(13), there are sufficiently accurate and less time-consuming semiemperical dependencies describing the thermal EOS. Among them, for instance, is the well-known Redlich-Kwong equation:

$$\left[p+\frac{a^*}{\sqrt{T}\upsilon(\upsilon+b^*)}\right](\upsilon-b^*)=RT, \tag{14}$$

where a^*=0.4278$R^2T_{cr}^{2.5}/p_{cr}$; b^*=0.0867RT_{cr}/p_{cr}; T_{cr} and p_{cr} are critical gas temperature and pressure. Please, note that $\upsilon=1/\rho$ is a specific volume here.

To construct a calorific EOS, the following base thermodynamics relations are used:

$$\varepsilon(p,T)=h(p,T)-p/\rho; \tag{15}$$

$$\mathrm{d}h=c_p\mathrm{d}T+\frac{\partial h}{\partial p}\mathrm{d}p, \tag{16}$$

where h is enthalpy, c_p is the specific heat capacity at constant pressure. If thermal EOS is known, parameter $(\partial h/\partial p)_T$ can be determined from the well-known thermodynamic relation:

$$\left(\frac{\partial h}{\partial p}\right)_T=-T\left(\frac{\partial \upsilon}{\partial T}\right)_p+\upsilon. \tag{17}$$

During the software implementation in a CFD-simulator, prior to fluid dynamics simulations, tabular function $\varepsilon=\varepsilon(p,T)$ is defined for the specified range of pressure and temperature. Integration of Eq.(16) is implemented by the Runge-Kutta method. For a CFD-simulator, the author and his co-workers generally use EOS Eqs.(14)~(15) (Seleznev *et al*., 2005a).

For numerical analysis of the set of Eqs.(1)~(12), we apply the integro-interpolation method by Samarsky for the construction of the difference equations, which, in essence, is a Russian analogue of the Finite Volume Method (FVM). To illustrate the parametric classes used for the difference equations, it is possible to present the class of the difference equations for a mathematical model of the non-isothermal transient motion of a multi-component gas mixture through a GPS line (see Eqs.(1)~(4) and (12)) (Seleznev *et al*., 2005a):

$$\left[(\rho F)^{(-S)}\right]_{\overset{+}{t}}+\left((\rho wf)_{(-R)}\right)_{\overset{+}{x}}^{(\sigma,\theta)}=0; \tag{18}$$

$$\left[(\rho F)^{(-S)}(Y_m)^{(-S)}\right]_{\overset{+}{t}}+\left((\rho wf)_{(-R)}(Y_m)_{(-R)}\right)_{\overset{+}{x}}^{(\sigma,\theta)}-\left[(\rho fD_m)_{(-R)}\delta(Y_m)^a\right]_{\overset{+}{x}}^{(\sigma,\theta)}=0, \tag{19}$$

$$m=1,...,N_S-1,\quad Y_{N_S}=1-\sum_{m=1}^{N_S-1}Y_m;$$

$$\left[(\rho F)^{(-S)}w^{(-S)}\right]_{t}^{+}+\left((\rho wf)_{(-R)}w_{(-R)}\right)_{x}^{(\sigma,\theta)+}$$
$$=-(B^{-}\gamma^{-}p_{\bar{x}}+B^{+}\gamma^{+}p_{x})^{(\sigma,\theta)}$$
$$-g\left[\rho\left(B^{-}\gamma^{-}(z_1)_{\bar{x}}+B^{+}\gamma^{+}(z_1)_{x}\right)\right]^{(\sigma,\theta)} \quad (20)$$
$$-\frac{\pi}{4}(\lambda\rho|w|r)^{(\sigma,\theta)}w^{(\sigma,\theta)};$$

$$\left[(\rho F)^{(-S)}\varepsilon^{(-S)}\right]_{t}^{+}+\left((\rho wf)_{(-R)}\varepsilon_{(-R)}\right)_{x}^{(\sigma,\theta)+}+K_t\left(\rho F\frac{w^2}{2}\right)$$
$$+K_x\left(\rho wf\frac{w^2}{2}\right)^{(\sigma,\theta)}=-\left((pwf)_{(-R)}\right)_{x}^{(\sigma,\theta)+}-g\left[\rho\left(B^{-}\gamma^{-}(z_1)_{\bar{x}}\right.\right.$$
$$\left.\left.+B^{+}\gamma^{+}(z_1)_{x}\right)\right]^{(\sigma,\theta)}w^{(\sigma,\theta)}-p^{(\sigma,\theta)}[F^{(-S)}]_{t}^{+}+(QF)^{(\sigma,\theta)}-\phi^{(\sigma,\theta)}$$
$$+\left[(kf)_{(-R)}\delta T^{a}\right]_{x}^{(\sigma,\theta)+}+\sum_{m=1}^{N_S}[(\rho D_m f)_{(-R)}(\varepsilon_m)_{(-R)}\delta(Y_m)^{a}]_{x}^{(\sigma,\theta)+};$$
(21)

$$\varepsilon_m=\varepsilon_m(\{S_{\text{mix}}\});\ m=1,...,N_S;\ T_1=T_2=...=T_{N_S};\quad (22)$$
$$p=p(\{S_{\text{mix}}\});\ \varepsilon=\varepsilon(\{S_{\text{mix}}\});\ k=k(\{S_{\text{mix}}\});$$

$$D_m=D_m(\{S_{\text{mix}}\}),\ m=1,...,N_S, \quad (23)$$

where F, B^{+}, B^{-} are the expressions approximating f; r is the expression approximating R (the type of these expressions is defined upon selection of a particular scheme from the class of schemes); s^a, s^b, r^a, r^b, σ, θ are parameters of the class of schemes (e.g., by specifying $s^a=s^b=1$, $r^a=r^b=0.5$, $\sigma=1$, $\theta=0$, a two-layer scheme with central differences is selected from the class of scheme, and by specifying $s^a=s^b=1$, r^a,r^b is according to the principles of "upwind" differencing, $\sigma=1$, $\theta=0$, is a two-layer "upwind" scheme (Seleznev *et al*., 2005a)); K_t and K_x are the differential-difference operators of functions $[\rho F(w^2/2)]$ and $[\rho wf(w^2/2)]$ over time and space, respectively (the type of these operators is defined upon selection of a particular scheme from the class of schemes); $\phi^{(\sigma,\theta)}$ is a difference expression approximating function $\Phi(T,T_{\text{am}})$. The difference Eqs.(18)~(23) are supplemented by difference expression of initial and boundary conditions, as well as of conjugation conditions.

To record the parametric class of the difference Eqs.(18)~(23), we used notations of a non-uniform space-time mesh $\{x_i,t_j\}$ (Fig.4), where x_i and t_j are coordinates of the mesh node numbered i over space, and j, over time, $i,j\in\mathbb{Z}$, $\mathbb{Z}$ being the set of nonnegative integers.

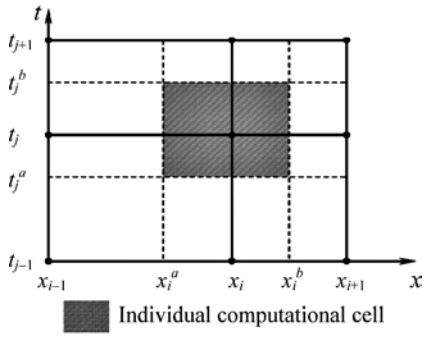

Fig.4 A space-time mesh (fragment)

To explain the notations, it is expedient to consider an individual computational cell (Fig.4) containing the node $\{x_i,t_j\}$ (mesh base node) and bounded by straight lines $x=x_i^a$, $x=x_i^b$, $t=t_j^a$ and $t=t_j^b$ ($x_{i-1}\le x_i^a\le x_i$, $x_i\le x_i^b\le x_{i+1}$, $t_{j-1}\le t_j^a\le t_j$, $t_j\le t_j^b\le t_{j+1}$, $x_i^a\ne x_i^b$, $t_j^a\ne t_j^b$). Let us introduce the so-called weighing parameters:

$$r_i^a=\frac{x_i^a-x_{i-1}}{x_i-x_{i-1}}=\frac{x_i^a-x_{i-1}}{h_i},\ r_i^b=\frac{x_i^b-x_i}{x_{i+1}-x_i}=\frac{x_i^b-x_i}{h_{i+1}},$$
$$s_j^a=\frac{t_j^a-t_{j-1}}{t_j-t_{j-1}}=\frac{t_j^a-t_{j-1}}{\tau_j},\ s_j^b=\frac{t_j^b-t_j}{t_{j+1}-t_j}=\frac{t_j^b-t_j}{\tau_{j+1}},$$

where $h_i=x_i-x_{i-1}$ and $h_{i+1}=x_{i+1}-x_i$ are steps "backward" and "forward" over the space coordinate for the i node; $\tau_j=t_j-t_{j-1}$ and $\tau_{j+1}=t_{j+1}-t_j$ are steps "backward" and "forward" over the time coordinate on the j time layer; $\alpha_i=h_{i+1}/h_i$ and $\beta_j=\tau_{j+1}/\tau_j$ are mesh parameters characterizing non-uniformity of the space and time mesh. To describe mesh function $y=y(x,t)$, the system Eqs.(18)~(23) uses the following notations:

$$y_i^j=y(x_i,t_j),\ y_i=y_i(t)=y(x_i,t),$$
$$y^j=y^j(x)=y(x,t_j).$$

where quadratic approximation is applied:

$$y(x,t)=a_i^{y-}(t)x^2+b_i^{y-}(t)x+c_i^{y-}(t),\ x\in[x_{i-1},x_i],$$
$$y(x,t)=a_i^{y+}(t)x^2+b_i^{y+}(t)x+c_i^{y+}(t),\ x\in[x_i,x_{i+1}],$$

the system uses the following notations:

$$\delta y(x,t)=\frac{\partial y}{\partial x}=2a_i^{y-}(t)x+b_i^{y-}(t),\ x\in[x_{i-1},x_i];$$

$$\delta y(x,t)=\frac{\partial y}{\partial x}=2a_i^{y+}(t)x+b_i^{y+}(t),\ x\in[x_i,x_{i+1}];$$
$$(\delta y^a)_i^j=2a_i^{y-}(t_j)x^a+b_i^{y-}(t_j),$$
$$(\delta y^b)_i^j=2a_i^{y+}(t_j)x^b+b_i^{y+}(t_j).$$

Also, the system Eqs.(18)~(23) uses the following index-free notations:

$$y=y_i^j,\ h=h_i,\ \alpha=\alpha_i,\ \tau=\tau_j,\ \beta=\beta_j,\ x=x_i,\ t=t_j,$$
$$\widehat{y}=y_i^{j+1},\ \breve{y}=y_i^{j-1},\ y(+1)=y_{i+1}^j,\ y(-1)=y_{i-1}^j,\ r^a=r_i^a,$$
$$r^b=r_i^b,\ s^a=s_j^a,\ s^b=s_j^b,\ i,j\in\mathbb{Z},$$
$$y^{(a)}=ay+(1-a)\breve{y},\ y^{(b)}=by+(1-b)y(-1),$$
$$y^{(a,b)}=a\widehat{y}+(1-a-b)y+b\breve{y},\ y^{(-S)}=s^a y+(1-s^a)\breve{y},$$
$$y^{(+S)}=s^b\widehat{y}+(1-s^b)y,\ y_{(-R)}=r^a y+(1-r^a)y(-1),$$
$$y_{(+R)}=r^b y(+1)+(1-r^b)y,\ y_{(-R)}(+1)=y_{(+R)},$$
$$y_{(+R)}(-1)=y_{(-R)},\ \widehat{y}^{(-S)}=y^{(+S)},\ \breve{y}^{(+S)}=y^{(-S)},$$
$$\Delta t^-=t-t^a=(1-s^a)\tau,\ \Delta t^+=t^b-t=s^b\widehat{\tau}=\beta s^b\tau,$$
$$\Delta x^-=x-x^a=(1-r^a)h,\ \Delta x^+=x^b-x=r^b h(+1)=\alpha r^b h,$$
$$\Delta t=t^b-t^a=\Delta t^++\Delta t^-=(1-s^a)\tau+s^b\widehat{\tau}$$
$$=(1-s^a)\tau+\beta s^b\tau,$$
$$\Delta x=x^b-x^a=\Delta x^+ +\Delta x^-=(1-r^a)h+r^b h(+1)$$
$$=(1-r^a)h+\alpha r^b h,$$
$$\gamma^-=\frac{\Delta x^-}{\Delta x}=\frac{(1-r^a)h}{(1-r^a)h+r^b h(+1)}=\frac{1-r^a}{(1-r^a)+\alpha r^b},$$
$$\gamma^+=\frac{\Delta x^+}{\Delta x}=\frac{r^b h(+1)}{(1-r^a)h+r^b h(+1)}=\frac{\alpha r^b}{(1-r^a)+\alpha r^b},$$
$$\delta y^a(+1)=\delta y^b,\ \delta y^b(-1)=\delta y^a,$$
$$y_x=\frac{y(+1)-y}{h(+1)},\ y_{\bar{x}}=\frac{y-y(-1)}{h},$$
$$y_{\bar{x}}(+1)=y_x,\ y_x(-1)=y_{\bar{x}},$$
$$y_{\underset{+}{t}}=\frac{\widehat{y}-y}{\Delta t},\ y_{\underset{+}{x}}=\frac{y(+1)-y}{\Delta x}.$$

For numerical analysis of the gas flow through a pipeline junction node Eqs.(5)~(11), it is possible to use the following difference equations (an expanded form, for reference see Fig.3b) (Seleznev *et al*., 2005a):

$$\frac{\rho_L^{j+1}-\rho_L^{j-1}}{(1+\beta_j)\tau_j}V-0.5\sum_{n=1}^{N}{}^{(n)}\rho_M^{j+1(n)}w_M^{j+1\,(n)}f_M^{j+1\,(n)}s=0;\quad(24)$$

$$V\left[\frac{\left(\rho_L^{j+1}+\rho_L^j\right)\left((Y_m)_L^{j+1}+(Y_m)_L^j\right)}{2(1+\beta_j)\tau_j}-\frac{\left(\rho_L^j+\rho_L^{j-1}\right)\left((Y_m)_L^j+(Y_m)_L^{j-1}\right)}{2(1+\beta_j)\tau_j}\right]$$
$$+0.5\sum_{n=1}^{N}\left\{{}^{(n)}f_L^{j+1}\left({}^{(n)}\rho_M^{j+1\,(n)}(D_m)_M^{j+1}+{}^{(n)}\rho_L^{j+1\,(n)}(D_m)_L^{j+1}\right)\cdot\frac{{}^{(n)}(Y_m)_L^{j+1}-{}^{(n)}(Y_m)_M^{j+1}}{2^{(n)}\Delta X}\right\}-0.25\sum_{n=1}^{N}\left\{\left({}^{(n)}(Y_m)_M^{j+1}+{}^{(n)}(Y_m)_L^{j+1}\right)\cdot{}^{(n)}s\,{}^{(n)}f_L^{j+1}\left({}^{(n)}\rho_M^{j+1\,(n)}w_M^{j+1}+{}^{(n)}\rho_L^{j+1\,(n)}w_L^{j+1}\right)\right\}=0;\quad(25)$$

$$\sum_{n=1}^{N}{}^{(n)}\rho_L\,{}^{(n)}w_L\,{}^{(n)}f_L\,{}^{(n)}s=0;\quad(26)$$

$${}^{(n)}V\left\{\frac{\left({}^{(n)}\rho_L^{j+1}+{}^{(n)}\rho_L^j\right)\left({}^{(n)}w_L^{j+1}+{}^{(n)}w_L^j\right)}{2(1+\beta_j)\tau_j}-\frac{\left({}^{(n)}\rho_L^j+{}^{(n)}\rho_L^{j-1}\right)\left({}^{(n)}w_L^j+{}^{(n)}w_L^{j-1}\right)}{2(1+\beta_j)\tau_j}\right\}+{}^{(n)}s\,{}^{(n)}f_L^{j+1}$$
$$\cdot\left({}^{(n)}\rho_L^{j+1\,(n)}(w_L^{j+1})^2-0.25\left[{}^{(n)}w_L^{j+1}+{}^{(n)}w_M^{j+1}\right]\cdot\left[{}^{(n)}\rho_L^{j+1\,(n)}w_L^{j+1}+{}^{(n)}\rho_M^{j+1\,(n)}w_M^{j+1}\right]\right)$$
$$=-\frac{{}^{(n)}f_L^{j+1}}{2}\left({}^{(n)}p_L^{j+1}-{}^{(n)}p_M^{j+1}\right){}^{(n)}s-\frac{\sqrt{\pi^{(n)}f_L^{j+1}}}{4}\cdot{}^{(n)}\lambda_L^{j+1\,(n)}\rho_L^{j+1\,(n)}w_L^{j+1}\left|{}^{(n)}w_L^{j+1}\right|{}^{(n)}\Delta X$$
$$-0.5\left({}^{(n)}(z_1)_L^{j+1}-{}^{(n)}(z_1)_M^{j+1}\right)g\,{}^{(n)}\rho_L^{j+1\,(n)}f_L^{j+1\,(n)}s;\quad(27)$$

$$V\frac{(\rho_L^{j+1}+\rho_L^j)(\varepsilon_L^{j+1}+\varepsilon_L^j)-(\rho_L^j+\rho_L^{j-1})(\varepsilon_L^j+\varepsilon_L^{j-1})}{2(1+\beta_j)\tau_j}$$
$$-0.25\sum_{n=1}^{N}\left\{{}^{(n)}f_L^{j+1}\left({}^{(n)}\rho_M^{j+1(n)}w_M^{j+1}+{}^{(n)}\rho_L^{j+1(n)}w_L^{j+1}\right){}^{(n)}s\cdot\left({}^{(n)}\varepsilon_M^{j+1}+{}^{(n)}\varepsilon_L^{j+1}\right)\right\}$$
$$=0.5\sum_{n=1}^{N}{}^{(n)}p_M^{j+1\,(n)}f_L^{j+1}\left({}^{(n)}w_M^{j+1}-{}^{(n)}w_L^{j+1}\right){}^{(n)}s+\sum_{n=1}^{N}\frac{\sqrt{\pi^{(n)}f_L^{j+1}}}{4}{}^{(n)}\lambda_L^{j+1\,(n)}\rho_L^{j+1}\left|{}^{(n)}w_L^{j+1}\right|^3{}^{(n)}\Delta X+Q_L^{j+1}V$$
$$-\sum_{n=1}^{N}\left[0.5\left({}^{(n)}k_M^{j+1}+{}^{(n)}k_L^{j+1}\right)\frac{{}^{(n)}T_L^{j+1}-{}^{(n)}T_M^{j+1}}{2^{(n)}\Delta X}{}^{(n)}f_L^{j+1}+{}^{(n)}\phi_L^{j+1\,(n)}\Delta X\right]-0.25\sum_{m=1}^{N_S}\sum_{n=1}^{N}\left\{\left({}^{(n)}(\varepsilon_m)_M^{j+1}+{}^{(n)}(\varepsilon_m)_L^{j+1}\right)\cdot{}^{(n)}f_L^{j+1}\left({}^{(n)}\rho_M^{j+1\,(n)}(D_m)_M^{j+1}+{}^{(n)}\rho_L^{j+1\,(n)}(D_m)_L^{j+1}\right)\right.$$

$$\cdot\frac{{}^{(n)}(Y_m)_L^{j+1}-{}^{(n)}(Y_m)_M^{j+1}}{2\cdot{}^{(n)}\Delta X}\Bigg\}+\sum_{n=1}^{N}{}^{(n)}\Bigg[\frac{w_L^{j+1}-w_L^{j-1}}{2(1+\beta_j)\tau_j}f_L\Delta X$$

$$\cdot\left(w_L^{j+1}-w_L^{j}\right)\left(\rho_L^{j}+\rho_L^{j-1}\right)\Bigg]. \qquad (28)$$

The last term of the difference Eq.(28) was introduced in order to stay on the conservative side Eq.(28).

In general, the difference Eqs.(18)~(28) are not less than first-order accurate (Seleznev *et al*., 2005a). Their unconditional stability is not denied (Seleznev *et al*., 2003). Higher-order accurate schemes for a CFD-simulator are described in detail in the monograph (Seleznev *et al*., 2005a). They were implemented in the CorNet software (and in its simplified special-purpose version AMADEUS) and Alfargus Pipeline Integrity and Information System. Algorithms for the simulation of GPS valve operation and description of GPS lines ruptures are described in (Seleznev *et al*., 2005a).

SIMULATION OF A CS BY MATHEMATICAL SOFTWARE OF A CFD-SIMULATOR

The principal task of mathematical simulation of stable and safe operation of a CFS is to determine physical parameters of gas at the CFS outlet on the basis of the known values of gas flow parameters at the CFS inlet. To construct a 1D mathematical model of a CFS in a CFD-simulator, we used a well-known polytropic model of a CFS developed by Stepanov. The model is based on the combination of analytical dependencies for polytropic fluid dynamics processes and empirical characteristics obtained for each CFS during its full-scale testing.

When simulating steady modes of CS operation, an isothermal model is used for description of the gas flow in a CGP and DC, and an isobaric model—for description of the gas flow in an ACD. The power drive is simulated by specifying an analytical dependency of the capacity at the CFS shaft on energy expenditures. Such approach provides for the simplicity of the conjugation of models and a high, from the practical standpoint, veracity of simulation.

As was noted above, a CFD-simulator of a particular CS is a result of combining GCU, ACD and DC models, by application of CGP models, into a single integral network model of the CS in accordance with the process flow charts of the actual CS (Fig.5).

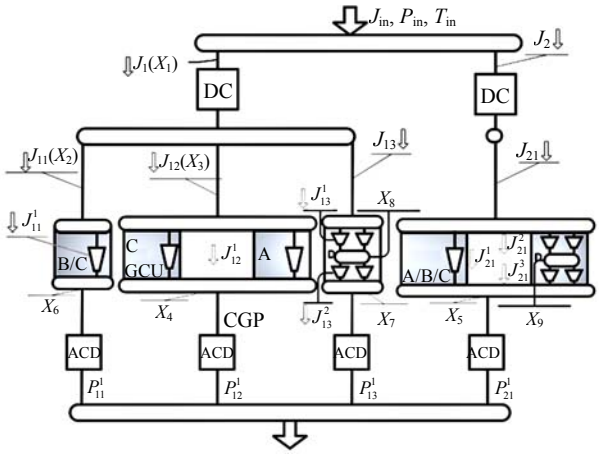

Fig.5 The scheme of decision independent variables assignment for on-line technological analysis of gas transmission through CS

In order to determine parameters of steady modes of natural gas transmission through a CS, generally, it is necessary to solve a system of nonlinear algebraic equalities under simple constraints on unknown variables. The system includes the law of conservation of gas masses at CGP branching points and one of the group of equations representing either conditions for conservation of mass flow rate at inflow and outflow CGPs in one branch, or conditions for equality of natural gas heads in parallel branches (Seleznev *et al*., 2005a), where a branch is a segment of a pipeline system, which comprises an inflow (inlet) CGP, CFS and an outflow (outlet) CGP (Fig.5).

As independent decision variables we use fractions of a mass flow rate of natural gas transmitted through separate branches of a CS, ratios of compression by compressor shops and ratios of compression by GCUs working as the first stage of transmitted gas compression at compressor shops. Such a set of variables allowed to reduce the problem of dimension and narrow the range of search for problem solution, by more accurate specification of constraints on variables. This allowed us to save considerable running time.

The mathematical model for the CS scheme presented in Fig.5 can be written as follows:

$$\begin{cases} P_{11}^{1}\left(J_{\text{in}},P_{\text{in}},T_{\text{in}},J_1(X_1),J_{11}(X_2),X_6\right) \\ \quad -P_{12}^{1}\left(J_{\text{in}},P_{\text{in}},T_{\text{in}},J_1(X_1),J_{12}(X_3),X_4\right)=0; \\ P_{12}^{1}\left(J_{\text{in}},P_{\text{in}},T_{\text{in}},J_1(X_1),J_{12}(X_3),X_4\right) \\ \quad -P_{13}^{1}\left(J_{\text{in}},P_{\text{in}},T_{\text{in}},J_1(X_1),J_{13},X_8,X_7\right)=0; \\ P_{13}^{1}\left(J_{\text{in}},P_{\text{in}},T_{\text{in}},J_1(X_1),J_{13},X_8,X_7\right) \\ \quad -P_{21}^{1}\left(J_{\text{in}},P_{\text{in}},T_{\text{in}},J_2,J_{21},X_9,X_5\right)=0; \\ J_{11}(X_2)-J_{11}^{1}(X_6)=0; \\ J_{12}(X_3)-J_{12}^{1}(X_4)=0; \\ J_{13}-J_{13}^{1}(X_8)=0; \\ J_{13}^{1}(X_8)-J_{13}^{2}(X_8,X_7)=0; \\ J_{21}-J_{21}^{1}(X_5)-J_{21}^{2}(X_9)=0; \\ J_{21}^{2}(X_9)-J_{21}^{3}(X_9,X_5)=0; \\ 0<X_i<1,\ i=1,2,3; \\ \varepsilon_{\max}^{1}<X_j<\varepsilon_{\max}^{\text{shop}},\ j=4,5,6,7; \\ \varepsilon_{\min}^{1}<X_k<\varepsilon_{\max}^{1},\ k=8,9, \end{cases} \tag{29}$$

where P_{11}^{1}, P_{12}^{1}, P_{13}^{1}, P_{21}^{1} are the natural gas pressure at the outlet of each of the CS branches, J_{in}, P_{in}, T_{in} are the natural gas flow rate, pressure and temperature at the CS inlet, J_1, J_2 are the natural gas mass flow rates through "branches I", J_{11}, J_{12}, J_{13}, J_{21} are the natural gas mass flow rates through "branches II", X_6, X_4, X_7, X_5 are the ratios of compression for compressor shops, X_8, X_9 are the ratios of compression for GCU groups of the first stages of compressor shops, $\varepsilon_{\min}^{1}/\varepsilon_{\max}^{1}$ is a minimal/maximal ratio of compression for GCU groups of the first stage, $\varepsilon_{\max}^{\text{shop}}$ is the maximal ratio of compression for compressor shops.

To assure a safe mode of CS operation, it is required to observe the following restrictions on: maximal volumetric capacity Q_j of each operating CFS; frequency u_j of the CFS shaft rotation; maximal capacity N_j of the CFS drive; maximal outlet pressure P_j of the CFS, which is determined by the pipe's strength; maximal temperature T_j at the CFS outlet, which is determined by the insulating coating; the lower value of pressure at the outlet of each CFS, is related to the requirements to maintain pressure at major gas tapping and boundary gas pipeline points. These restrictions can be formulated as one-sided and two-sided weak inequality:

$$\begin{cases} Q_j^{\min}\le Q_j(\boldsymbol{X})\le Q_j^{\max}; \\ u_j^{\min}\le u_j\le u_j^{\max}; \\ N_j(\boldsymbol{X})\le N_j^{\max}; \\ P_j^{\min}\le P_j(\boldsymbol{X})\le P_j^{\max}; \\ T_j(\boldsymbol{X})\le T_j^{\max}, \end{cases} \tag{30}$$

where index j=1,…,M means the number of CFS. Also, it is necessary to comply with restrictions on: positions of operational points at the CFS performance curves, related to surge-free operation requirements; conditions related to CFS drive's stable operation; etc. Compliance with the latest restrictions can only be analyzed via a detailed simulation of the mode of gas transmission through the CS.

The system of nonlinear algebraic inequalities Eq.(30) describes technological, operating and design constraints on CS equipment operation. When formulating the constraints in a CFD-simulator, maximum consideration is given to the specifics of the CS process flow chart and the modes of its operation, including a possibility of surging in "CFS—Adjacent CGP" (Seleznev *et al*., 2005a).

The resultant system Eqs.(29) and (30) represents a generalized system of nonlinear algebraic equalities and inequalities. One of the methods to solve the system of nonlinear algebraic equalities and inequalities is the well-known Interior Point Method, which, in a CFD-simulator, is implemented by statement and solution of an equivalent problem of mathematical optimization (Seleznev *et al*., 2005b). The equivalent optimization problem is solved by the method of modified Lagrange functions. If no solution can be found, the possibility of failure occurrence is admitted. The method we use makes it possible to identify constraints which are not complied with and to evaluate the extent of such non-compliance.

ON THE ADEQUACY OF GTN SIMULATION BY A CFD-SIMULATOR

To estimate the adequacy of simulation, we compared numerical simulation results and on-site measurements taken during the CFD-simulator's operation at actual GTNs (Tirpak *et al*., 2003). As an example, it is worth noting that relative errors in

calculations for pressure of natural gas transmission through a GPS that occurred during three years of AMADEUS CFD-simulator's operation at the SPP International Company have not exceeded 2.7% (0.18 MPa in magnitude). Relative errors in calculations of temperature of the transmitted gas have not exceeded 0.7% (1.9 K). Deviations of data, which were calculated for mass flow rate of transmitted gas, from meter readings have not exceeded 6.3% (94.0 kg/s in magnitude).

CONCLUSION

The approach presented in this article for high-accuracy numerical analysis of operating parameters of industrial pipeline networks using CFD-simulators is based on adaptation of the full system of equations of fluid dynamics to conditions of transient, non-isothermal processes of the flow of gas mixtures in actual GTNs. The adaptation applies the rule of minimization of the number and depth of accepted simplifications and assumptions. The high accuracy of analysis of industrial pipeline networks operating parameters is understood here as the most reliable description and prediction of actual processes in a GTN, which are achievable due to the present level of development of mathematical modeling and technical monitoring methods and available computer hardware. Development and operation of CFD-simulators in solving industrial problems of improving safety, efficiency and environmental soundness of pipeline network operation can be regarded as one of the promising trends of industrial application of the state-of-the-art computational mechanics methods.

References

Kinsman, P., Lewis, J., 2000. Report on a Study of International Pipeline Accidents. Prepared by Mechphyic Scientific Consultants for the Health and Safety Executive. Contract Research Report 294/2000, HSE, UK, p.128.

Seleznev, V., Aleshin, V., 2004. Computation Technology for Safety and Risk Assessment of Gas Pipeline Systems. Proceedings of the Asian International Workshop on Advanced Reliability Modeling (AIWARM'2004), Japan. World Scientific Publishing Co. Pte. Ltd., London, UK, p.443-450.

Seleznev, V., Pryalov, S., Kiselev, V., 2003. Theory and Application Experience of Computer Computation Fluid Dynamic Simulators of Gas Mixture Transportation at Industrial Pipeline Networks. Proceeding of Sixth ISTC Scientific Advisory Committee and Russian Academy of Sciences Seminar "Science and Computing", Russia, **I**:213-220.

Seleznev, V.E., Aleshin, V.V., Klishin, G.S., Il'kaev, R.I., 2005a. Numerical Analysis of Gas Pipelines: Theory, Computer Simulation, and Applications. KomKniga, Moscow, p.720.

Seleznev, V.E., Kiselev, V.V., Zelenskaya, O.I., 2005b. Failure Forecast in Engineering Systems by Searching for the Interior Points of System of Algebraic Equalities and Inequalities. Proceeding of the European Safety and Reliability Conference (ESREL-2005), Taylor & Francis Group, London, **II**:1773-1776.

Tirpak, M., Marko, J, Heringh, A., Seleznev, V.E., Pryalov, S.N., Kiselev, V.V., 2003. Experiences with Real Time Systems and Their Contribution to Safe and Efficient Control of Gas Transport System. Papers Book at 35 Annual Meeting of the Pipeline Simulation Interest Group (PSIG-2003), Switzerland, p.1-8.

True, W.R., 2001. Regulatory actions loom for US pipelines in 2001. *Oil & Gas Journal*, **99**(1):70-71.